Edge Recombination Analysis of Silicon Solar Cells Using Photoluminescence Measurements

Hannah Stolzenburg[1, a)], Andreas Fell[1], Florian Schindler[1], Wolfram Kwapil[2], Armin Richter[1], Puzant Baliozian[1] and Martin C. Schubert[1]

[1]*Fraunhofer Institute for Solar Energy Systems ISE, Heidenhofstraße 2, 79110 Freiburg, Germany*
[2]*University Freiburg, Department of Sustainable Systems Engineering (INATECH), Emmy-Noether-Str. 2, 79110 Freiburg, Germany*

[a)] Corresponding author: hannah.stolzenburg@ise.fraunhofer.de

Abstract. Edge losses in silicon solar cells are becoming more important in current photovoltaic research, especially in shingled cell modules with high perimeter to area ratios. Hence, in this study a new approach is presented to quantify edge recombination losses by using photoluminescence (PL) measurements combined with device modelling. The main focus of this work is to determine and separate the contribution of the two relevant edge recombination losses: (i) recombination at the bulk edge, described by an effective surface recombination velocity $S_{\mathrm{eff,edge}}$, and (ii) recombination at the pn-junction edge, described by an edge-length specific non-ideal recombination parameter $J_{02,\mathrm{edge}}$. For this purpose, the PL gradient towards the edge at different illumination intensities is fitted by Quokka3 simulations. The developed method is applied for differently separated unpassivated edges, namely by thermal laser separation (TLS) and by mechanical cleaving. Additionally, an emitter window for the TLS edge is introduced where no pn-junction at the edge is present. It was found that the emitter window results in less edge recombination while having the same bulk-edge recombination properties as without. As a result, $J_{02,\mathrm{edge}}$ = 3 nA/cm and $S_{\mathrm{eff,edge}}$ = 10^5 cm/s are determined for the TLS edge without emitter window while the mechanically cleaved edge showed higher edge recombination.

INTRODUCTION

One possibility to increase the power density of solar modules is the use of half cells [1] or the shingling of cells [2,3]. Whereas this approach offers significant advantages like lower series resistances and in the case of shingled cells also less shadowing, a disadvantage is that the perimeter to area ratio rises. Hence, losses at the edges have a greater impact on the solar cell performance, and it is therefore expected that the impact is especially high for high efficiency cells like passivated emitter and rear cells (PERC), cells with tunnel oxide passivated contacts (TOPCon) or hetero junction cells (HJT).

In the last years, the investigation of the edge recombination mainly focused on its influence on the global IV parameters. For instance, it could be found that edge recombination results in a drop in the fill factor (*FF*) and open-circuit-voltage (V_{oc}) [2,4–7]. However, these studies required extensive sample processing (e.g. variation of the perimeter to area ratio) and revealed only indirect evidence for the edge contribution to the solar cell performance. It is therefore our main goal to develop spatially resolved methods to more directly quantify edge-related losses without the need for further process variations and to gain a more detailed understanding of the edge recombination.

Following the model in [8] where the locality of the edge recombination is accounted for by using multidimensional device simulations, the aim of the present work is to differentiate between the two dominating edge recombination losses depicted in Fig. 1b: (i) recombination at the bulk edge, described by an effective surface recombination velocity $S_{\mathrm{eff,edge}}$, and (ii) recombination at the edge of the pn-junction, described by an edge-length specific non-ideal recombination parameter $J_{02,\mathrm{edge}}$ [8,9]. Notably, those two recombination properties are not strictly

dependent on each other [3]. Therefore, both need to be characterized unambiguously to conduce to a better understanding of the source of edge recombination for eventually optimizing the edge properties of solar cells.

In this study, a characterization method based on photoluminescence imaging (PLI) and multidimensional device simulation is developed, which is exemplarily demonstrated for a diffused and surface passivated wafer. For this purpose, edges which are differently affected by edge recombination are chosen. This is achieved by different edge preparation methods, namely thermal laser separation (TLS) [10] with or without an emitter window (i.e. the emitter does not reach the edge) and mechanical cleaving (see also Fig. 1a). By fitting the PL gradient towards the edges, simulated with Quokka3 [11] to experimental PLI measurements using non-linear least squares, $S_{\mathrm{eff,edge}}$ and $J_{02,\mathrm{edge}}$ can be determined.

SAMPLE PREPARATION

The schematic top view and cross section of the investigated sample system is shown in Fig. 1a and 1b, respectively. 1 Ωcm n-type FZ wafers featuring a boron-diffused front side emitter (90 Ω/sq) passivated with an ALD Al_2O_3 / PECVD SiN_x stack (10 nm/60 nm) and a PECVD SiN_x rear side passivation (70 nm). Further, the 6 inch wafer is planar with a thickness of 250 µm.

Samples with three differently processed wafer edges were investigated (Fig. 1a): (i) the wafer is separated by TLS [10] through the emitter from the front side, (ii) by TLS with a distance d_{EW} of 300 µm between the emitter and the edge (Fig. 1b) and (iii) by diamond scribing and subsequent manual mechanical cleaving through the emitter also from the front side.

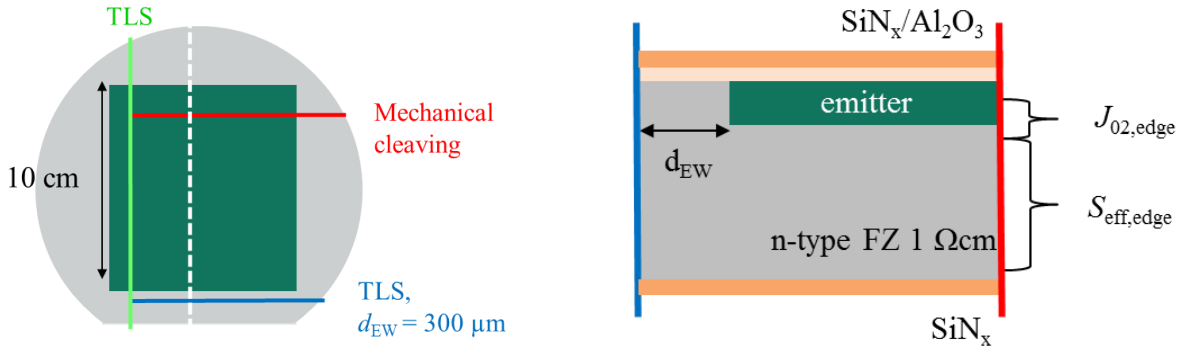

(a) (b)

FIGURE 1. (a) Top-view sketch of the 6 inch wafers with emitter window (dark green) and indicated edge types (colored); (b) cross-section sketch (white dotted line in Fig. 1a) where the distance between emitter and edge is indicated by the parameter d_{EW}.

METHOD DEVELOPMENT

Photoluminescence Imaging

To measure the spatially resolved PL intensity, the wafers were illuminated by an 808 nm laser at six different illumination intensities corresponding to 0.02-1 sun. To reduce blurring effects due to photon scattering in the wafer and the detector, 1000 and 1050 nm short pass filters are mounted. In Fig. 2a the PL image at 0.97 suns of the sample with the three studied edges is shown. Averaging line-scans of the PL signal as depicted in Fig. 2a for the TLS edge through emitter, the influence of the edge recombination is evident for all illumination intensities, shown in Fig. 2b. As explained in [5] by Hermle et al., the fraction of pn-junction recombination to bulk recombination gets higher for lower illumination intensities due to the relation between excess charge carrier concentration Δn and doping level. A closer look at the profiles reveals a PL decrease on a longer local range at lower illumination

intensities. A homogeneous plateau is approximately reached at 30 mm distance of the edge for low illumination intensities.

Hence, the influence of edge recombination for the differently prepared edges is best visible at low intensities. The PL image at 0.02 suns in Fig. 3a and the corresponding PL profiles in Fig. 3b clearly show a distinction between the differently processed edges. In opposition to the mechanically cleaved and the TLS edge with emitter window, the TLS edge without emitter window shows some inhomogeneities. Since they were not visible after separation, PL regions which are least affected by inhomogeneities were chosen for the analysis.

As a result, on the one hand, the TLS cleaved edge through the emitter is not as affected by edge recombination as the mechanically cleaved edge which is also true for the averaged signal over the whole edges and, on the other hand, the expected positive influence of an emitter window [9,12] due to the missing conductivity of minority carriers through the emitter to the edge is observed.

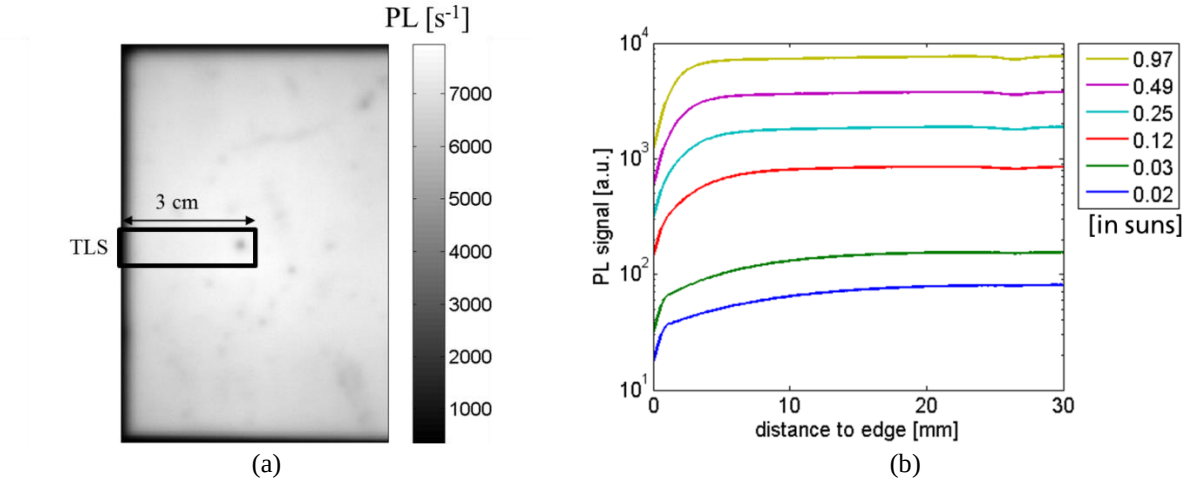

FIGURE 2. (a) PL image at 0.97 suns; (b) PL profiles at six different illumination intensities for the TLS separation through the pn-junction.

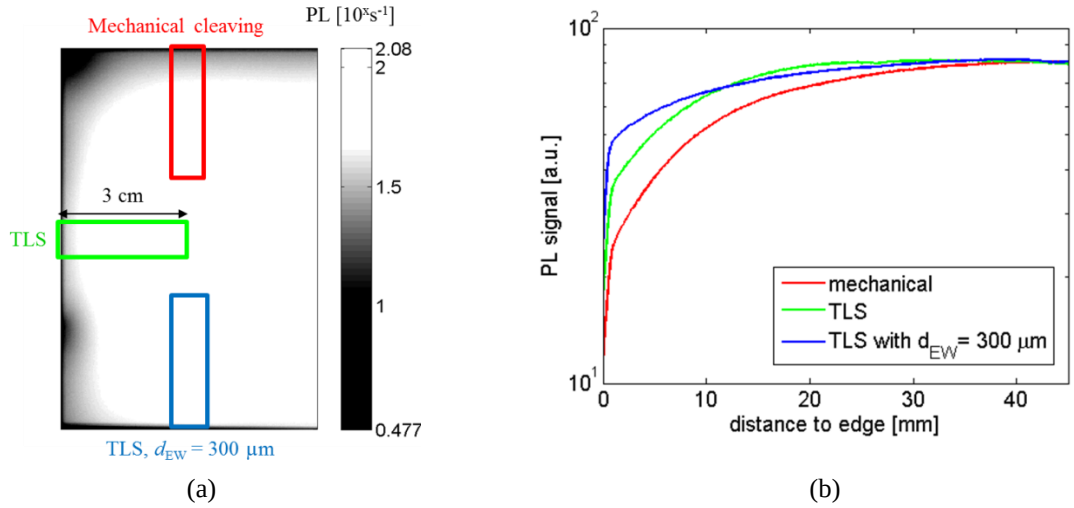

FIGURE 3. (a) Logarithmically scaled PL image at 0.02 suns shows the three differently affected edges and (b) the corresponding PL profiles averaged over the respective areas depicted by the rectangles.

Quantification of Edge Recombination

For the quantification of the edge recombination multidimensional PL simulations using Quokka3 are fitted to the experimental PL data. In the first step, the simulation is calibrated within three homogeneous areas of the wafer which are not influenced by the edges. Therefore, the effective lifetime curve in dependence on the excess charge carrier density Δn is fitted, see Fig. 4a. For this purpose, the experimental data are obtained from PL imaging calibrated by harmonically modulated PL [13]. By adjusting the simulated curve, an emitter recombination current J_{0e} = 70 fA/cm^2 as well as midgap related bulk lifetimes $\tau_{p0,bulk}$ = 1.5 ms and $\tau_{n0,bulk}$ = 50 ms are fitted while recombination at the rear is negligible. Furthermore, an illumination intensity scaling factor is determined, see Fig. 4b, considering the optics of the PL-setup in the simulations and all six illumination intensities concurrently.

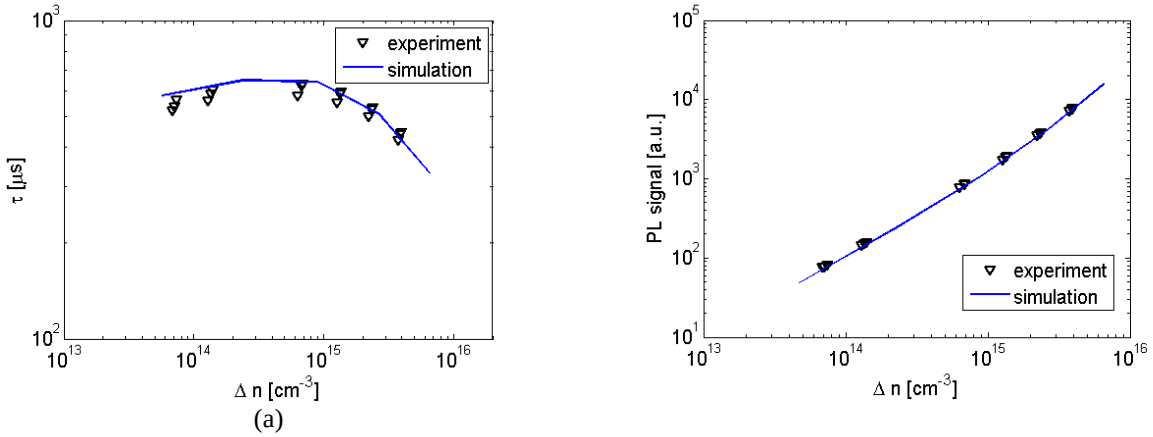

(a)

FIGURE 4. (a) Excess charge carrier density Δn dependent effective lifetime τ curve whereas three homogeneous spots in the middle of the wafer which are not the influenced by the edge are chosen. The fit parameters of the simulation are J_{0e} = 70 fA/cm^2, midgap related bulk lifetimes $\tau_{p0,bulk}$ = 1.5 ms and $\tau_{n0,bulk}$ = 50 ms; (b) calibration of the PL intensity.

After the calibration, the PL signal towards the edges from 2D simulations including the edge can be fitted to the corresponding experimental data. To increase the distinguishability of the $S_{eff,edge}$ and $J_{02,edge}$ values, the six illumination intensities are fitted simultaneously by finding the minimal reduced χ_{red}^2, i.e. using non-linear least squares per degrees of freedom weighted with an experimental error of 10% of the PL signal. In Fig. 5, a selected set of simulation profiles in the fit parameter range is compared to the TLS edge profile (through the emitter) for three different illumination intensities. Obviously, $J_{02,edge}$ and $S_{eff,edge}$ are differently dependent on the illumination intensities whereas the $J_{02,edge}$ contribution is more dominant on low illumination intensities. The best match of simulation and experiment for the TLS edge through the emitter is received for $J_{02,edge}$ = 3 nA/cm and $S_{eff,edge}$ = 10^5 cm/s. Hence, due to the different dependencies of $J_{02,edge}$ and $S_{eff,edge}$ on the excess charge carrier density, i.e. different illumination intensities, the reliability in distinguishing $J_{02,edge}$ and $S_{eff,edge}$ increases by fitting all the illumination intensity profiles concurrently. In Fig. 6a the perfect agreement between simulation and experiment is visible. In addition to that, the emitter window with d_{EW} = 300 µm at the TLS edge is simulated, which is also in good agreement with the experimental data, see Fig. 6b. Since for a present emitter window only an influence of $S_{eff,edge}$ is assumed, a good fit with the same $S_{eff,edge}$ as without emitter window is a good consistency check for the distinguishability of $J_{02,edge}$ and $S_{eff,edge}$.

The best fit results for the edge recombination parameters of the TLS and mechanically cleaved edge as well as the corresponding minimal χ_{red}^2 are listed in Tab. 1. The higher χ_{red}^2-values for the TLS edge with emitter window and mechanically cleaved edge without emitter window are due to some additional long-range PL decrease. The resulting $J_{02,edge}$ and $S_{eff,edge}$ values lead to the conclusion that for both, the mechanically cleaved and TLS edge, the worst-case assumption with $J_{02,edge}$ = 19 nA/cm and $S_{eff,edge}$ = 10^6 cm/s, according to the simulation study in [8], is too high. However, the edge recombination velocity for the mechanically cleaved edge is with $S_{eff,edge}$ = 10^6 cm/s comparable with the reported values in [3,5,8] for an unpassivated edge. The so far reported $J_{02,edge}$-values calculated from fitting dark-IV-curves like in [5,6] show mostly higher values than in this study while Rühle et al. [12] also reported 5 nA/cm for a mechanically unpassivated edge.

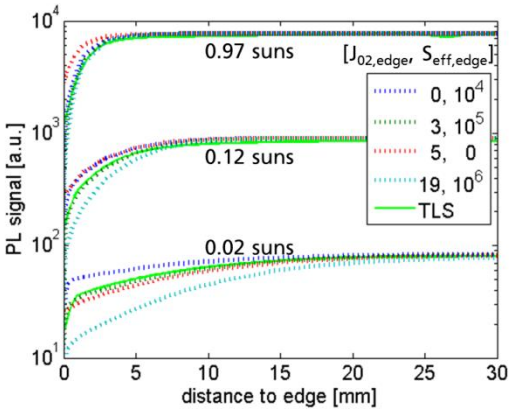

FIGURE 5. Comparison of the experimental data of the TLS edge through emitter at 0.02, 0.12 and 0.97 suns with a selected set of simulation profiles varying $J_{02,edge}$ [nA/cm] and $S_{eff,edge}$ [cm/s].

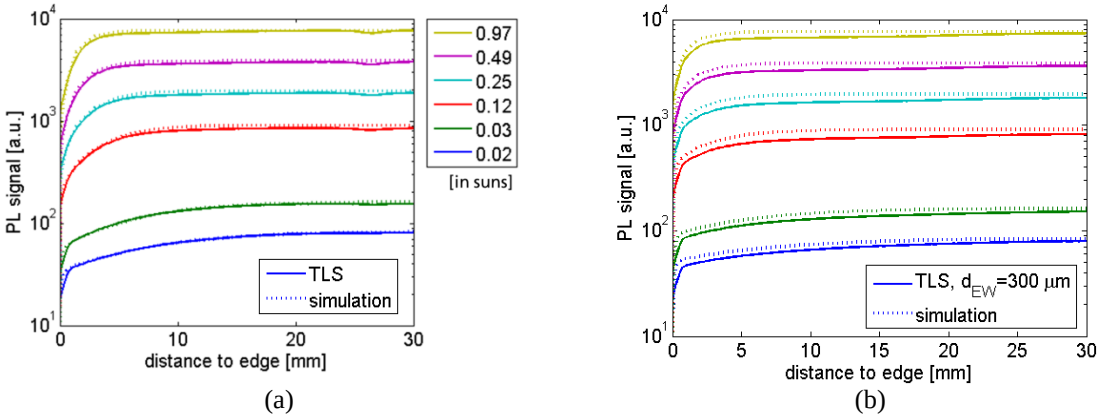

FIGURE 6. Comparison of the experimental and simulated data of the TLS edge using the best-fit, which is shown for all six illumination intensities in (a) for the TLS edge with $J_{02,edge}$ = 3 nA/cm and $S_{eff,edge}$ = 10^5 cm/s and in (b) for the TLS edge with emitter window with $S_{eff,edge}$ = 10^5 cm/s.

TABLE 1. Best fitting parameters for the different edges types.

Edge	$J_{02,edge}$ [nA/cm]	$S_{eff,edge}$ [cm/s]	χ_{red}^2
TLS	3	10^5	0.62
TLS (d_{EW} = 300 µm)	-	10^5	2.06
Mechanical cleaving	5	10^6	2.27

CONCLUSION

In this study a new characterization method is presented to quantify the edge recombination by comparing PL measurements with Quokka3 device simulations, sensitive to differently processed edges. By fitting simulated to measured PL profiles towards the edges, an $J_{02,edge}$ and $S_{eff,edge}$ could be determined. It was found that the emitter window results in less edge recombination while having the same bulk-edge recombination properties as without. While taken also the different dependencies on illumination intensities of the two edge recombination parameters into account, the distinguishability of $J_{02,edge}$ and $S_{eff,edge}$ is improved. Hence, the developed method can be applied for extracting detailed information about the edges. Since the overall goal is to optimize silicon solar cell performance, the comparison of mechanical cleaving and TLS lead to the conclusion that the TLS processed edge causes less edge losses and is therefore a promising separation method for shingled cells.

Developing the presented method further, inhomogeneities of wafers and optical artifacts of the PL-setup have to be investigated in more detail. Since the method is not constrained to specific sample parameters, it can be applied for different high-efficieny silicon solar cells to obtain detailed information about the edge losses in silicon solar cells.

ACKNOWLEDGMENTS

They also acknowledge the funding of the German Federal Ministry for Economic Affairs and Energy (BMWi) in the frame of the project “PV-BAT400” under contract number 0324145.

REFERENCES

1. S. Zhang, X. Pan, H. Jiao, W. Deng, J. Xu, Y. Chen, P. P. Altermatt, Z. Feng, and P. J. Verlinden, IEEE J. Photovoltaics **6**, 145-152 (2016).
2. S. W. Glunz, J. Dicker, M. Esterle, M. Hermle, J. Isenberg, F. J. Kamerewerd, J. Knobloch, D. Kray, A. Leimenstoll, F. Lutz, D. Osswald, R. Preu, S. Rein, E. Schaffer, C. Schetter, H. Schmidhuber, H. Schmidt, M. Steuder, C. Vorgrimler, and G. Willeke, “High-efficiency silicon solar cells for low-illumination applications,” in *Conference Record of the Twenty-Ninth IEEE Photovoltaic Specialists Conference, 2002* (IEEE, 2002), pp. 450-453.
3. N. Woehrle, E. Lohmueller, M. Mittag, A. Moldovan, P. Baliozian, T. Fellmeth, K. Krauss, A. Kraft, and R. Preu, Photovoltaics International **36**, 48-62 (2017).
4. J. H. Guo, J. E. Cotter, K. R. McIntosh, K. C. Fisher, F. W. Chen, and A. Karpour, "Edge passivation for small-area, high efficiency solar cells," in *Proceedings of the 22nd EU-PVSC*, (Milan, 2007), pp. 1348–1351.
5. M. Hermle, J. Dicker, W. Warta, S. W. Glunz, and G. Willeke, "Analysis of edge recombination for high-efficiency solar cells at low illumination densities," in *3rd World Conference on Photovoltaic Energy Conversion, 2003*, Proceedings of. Vol. 2 (IEEE, Osaka, 2003), pp. 1009-1012.
6. K. R. McIntosh and C. B. Honsberg, "The influence of edge recombination on a solar cell's IV curve," in *Proc. 16th PVSEC*, (Glasgow, 2000), pp. 1651-1654.
7. R. Kuehn, P. Fath, and E. Bucher, "Effects of pn-junctions bordering on surfaces investigated by means of 2D-modeling," in *Conference Record of the Twenty-Eighth IEEE Photovoltaic Specialists Conference-2000*, Proc. 28th IEEE PVSEC, (IEEE, 2000), pp. 116-119.
8. A. Fell, J. Schoen, M. Mueller, N. Woehrle, M. C. Schubert, and S. W. Glunz, IEEE J. Photovoltaics **8**, 428-434 (2018).
9. N. Woehrle, T. Fellmeth, E. Lohmueller, P. Baliozian, A. Fell, and R. Preu, "The SPEER solar cell - simulation study of shingled bifacial PERC-technology-based stripe cells," in *33rd European Solar Energy Conference and Exhibition*, (2017), pp. 844-848.
10. H.-U. Zuehlke, G. Eberhardt, and P. Mende, "TLS-Dicing-the way to higher yield and throughput," in *2008 International Symposium on Semiconductor Manufacturing (ISSM)*, (IEEE, 2008), pp. 301-304.
11. A. Fell, J. Schoen, M. C. Schubert, and S. W. Glunz, Sol. Energy Mater. Sol. Cells **173**, 128-133 (2017).
12. K. Ruehle, M. K. Juhl, M. D. Abbott, L. M. Reindl, and M. Kasemann, IEEE J. Photovoltaics **5**, 1067-1073 (2015).
13. J. A. Giesecke, M. C. Schubert, B. Michl, F. Schindler, and W. Warta, Sol. Energy Mater. Sol. Cells **95**, 1011-1018 (2011).